Data from GNSS-Based Passive Radar to Support Flood Monitoring Operations

Data from GNSS-based passive radar to support flood monitoring operations

Rayan Imam
Dept. of Electronics and Telecommunications
Politecnico di Torino
Torino, Italy
rayan.imam@polito.it

Marco Pini
Navigation Technologies Research Area
LINKS Foundation
Torino, Italy
Marco.Pini@linksfoundation.com

Gianluca Marucco
Navigation Technologies Research Area
LINKS Foundation
Torino, Italy
Gianluca.Marucco@linksfoundation.com

Fabrizio Dominici
Mobile Solutions Research Area
LINKS Foundation
Torino, Italy
Fabrizio.Dominici@linksfoundation.com

Fabio Dovis
Dept. of Electronics and Telecommunications
Politecnico di Torino
Torino, Italy
fabio.dovis@polito.it

***Abstract*—Signals transmitted by Global Navigation Satellite Systems can be exploited as signals of opportunity for remote sensing applications. Satellites can be seen as spread sources of electromagnetic radiation, whose signals reflected back from ground can be processed to detect and monitor geophysical properties of the Earth's surface. In the past years, several experiments of GNSS-based passive radars have been demonstrated successfully, mainly from piloted aircraft. Then, the proliferation of small UAVs enabled new applications where GNSS-based passive radars can provide useful geospatial information for environmental monitoring. Thanks to the availability of commercial Radio Frequency front ends and the enhanced processing capabilities of embedded platforms, it is possible to develop GNSS-based passive radars at moderated cost. These can be mounted on Unmanned Aerial Vehicles, and be used to support the sensing of environmental parameters. This paper presents the results of an experimental campaign based on the use of a UAV for GNSS reflectometry, tailored to the detection of the presence of water on ground after floods. The work is part of wider project, which intends to develop solutions to support rescuers and decision makers to manage operations after natural disasters, through the integration and modelling of geospatial data coming from multiple sources.**

***Index Terms*—GPS, passive radar, UAVs, geospatial data, flood monitoring, signals of opportunity**

I. Introduction

The great positive impact of Unmanned Aerial Vehicles (UAV) on modern society is confirmed by their increasing diffusion for a widespread set of services. Beyond the military use, they offer a broad range of solutions for many civil applications, such as security and surveillance, critical infrastructures diagnostic, monitoring of environmental pollution and recognitions after natural disasters. Commercial UAVs are cost-effective with respect to piloted light aircraft, especially considering that they can be equipped with different types of sensors, like optical and hyperspectral cameras, sensors for environmental parameters, Synthetic Aperture Radar (SAR), Inertial Measurement Unit (IMU) and Global Navigation Satellite System (GNSS) receivers. The possibility to be a platform for diverse sensors expanded GNSS original fields of application and, among all the disciplines, GNSS-Reflectometry (GNSS-R) is certainly one which benefited from the UAVs' diffusion. GNSS-R allows for monitoring parameters of the Earth's surface, by processing GNSS signals backscattered from ground [1]. The concept is rather simple: the GNSS satellite is the transmitter and together with a receiver capable of processing reflected GNSS signals can be seen as a passive radar. The wide range of application of this concept has been presented in literature for different purposes: altimetry [2] [3], water basins detection and wind retrieval [4], to monitor the presence of vegetation [5], to estimate ice/snow thickness [6], to estimate the surface roughness [7], and to measure the soil moisture [8]–[10] and ocean wave height [11], [12]. More recently, the soil moisture retrieval, which consists in measuring the soil dielectric constant, i.e. the relative permittivity, is becoming an increasingly popular application, as outlined in [13] and [14].

GNSS-R from commercial UAV asks for the review of the conventional hardware employed in the first experiments using piloted aircraft, because the reduction of size, weight and power consumption is fundamental, especially if the experiment is carried out with small commercial quad- or hex-copters. This was proposed in [15] , where a miniaturized receiver was presented. The design was based on two GPS L1 front ends with a common clock, connected to a Universal Serial Bus (USB) bridge for high-speed data transfer. A Nano-ITX Single Board Computer (SBC) was used to store in memory raw signal samples, which were analysed in post-processing. In [16] an FPGA-based GNSS reflectometer was designed to compute the full two-dimensional Delay Doppler Maps (DDMs), with update rate of 1 ms and performing coherent and incoherent averaging. Most of existing GNSS-

based passive radars consist of a Right Hand Circular Polarized (RHCP) antenna pointing at the zenith and another pointing at nadir for the reception of ground reflected signals. This last can be Left Hand Circular Polarized (LHCP), assuming that the reflection causes a complete polarization flip, or dual polarized.

In this work we present the results obtained with a simplified version of the sensor introduced in [17]. It features a compact design and uses a LHCP antenna to receive ground reflected signals. Raw samples are stored in files for post-processing purposes, with a size limit that corresponds to a flight duration of approx. 30 minutes. However such a duration was considered more than enough for the objective of the experiment, which wanted to demonstrate GNSS-R as a valid supporting techniques for the monitoring of water surface after floods.

II. MOTIVATION OF THE WORK

The objective of the work presented in this paper was twofold:

1) Investigate the possibility to add additional capabilities to small UAVs, as they are valuable instruments when satellite-based imagines are not yet available and can provide useful data of flooded areas for post-mission assessments.
2) Assess the performance of the GNSS-based passive radar [17], made of low cost commercial components, when it is mounted on board of a small UAV and used to monitor water surfaces on ground. Such an assessment could enable a further source of geospatial data in the system under development in the I-REACT project [18], which proposes solutions to improve the response of rescuers and decision makers to extreme events.

This paper presents the results of the analysis performed on several data sets, which were collected with a GNSS-based passive radar mounted on a hexa-copter and employed to detect and monitor water surfaces. Section III describes the hardware components integrated into the UAV, providing insights on the methodology followed during the data collections and the following post processing analysis. Based on the first sections, Section IV discusses the most important results, which have been divided in two different study cases for the sake of simplicity. Finally, Section 5 concludes the paper, remarking the value of data from GNSS-based passive radars for environmental studies.

III. UAV-BASED DATA COLLECTIONS AND PROCESSING

In order to demonstrate the feasibility of the detection of water surfaces with low cost devices suitable to be carried by small UAVs, we prepared a flying prototype able to receive and store onboard GNSS radio frequency signals both direct and reflected. This was done using two different antennas: the first pointing upwards, the second downwards. This is an essential feature of the radar: the synchronous recording of the two signals enables an accurate geo-referencing of measurements, which is fundamental in post mission analysis.

The targeting of water surfaces was done in post processing aiming at optimizing all the parameters involved and consequently improve results reliability. All GNSS signals have a carrier frequency of the order of 1 GHz (1.150 - 1.620 GHz) and are transmitted with RHCP. When they are reflected by a smooth surface, their polarization is reversed, becoming LHCP. Therefore, in order to maximize the signal power to be captured and to discriminate between RHCP and LHCP signals, it is necessary to use proper antennas able to selectively receive the two kind of polarization. In the case of non-specular surfaces, the reflected signal will be a mix of the two components being the LHCP the most relevant.

A. Experimental system set up

This section describes the preparatory work carried out to collect data with a hexa-copter operated by means of a remote controller. The work started from a pre-existing prototype [17] that was conceived to fly under the wing of a piloted aircraft and to be part of a payload requiring specific interfaces for mounting, power supply and control. In this case, the objective was to exploit the same principles using an affordable equipment also able to simplify logistics, ease activities, and increase monitoring possibilities in emergency scenarios. These were the main reason behind the choice of a UAV.

The carrier change requested a number of conceptual and functional modifications of the GNSS-based passive radar to address the weight requirement. The UAV pilot set a target weight of 700 grams. Therefore, we decided to mount a light LHCP antenna downwards, the RF front end was kept simple, having only one channel for the processing of the reflected signal. The downwards antenna was placed just underneath the cradle and was provided with an aluminum ground plane with a diameter of 10 cm [19]. On the other hand, the upwards antenna was mounted on top of sort of a tripod with its ground plane.

The second aspect considered was the power supply of the device. In order to avoid the exploitation of the on-board power supply, a single 7.4 V Li-Polymer battery was mounted to provide power to both the RF front end and the single board computer used to log data. The front end was connected directly to the battery (accepting power ranging from 5 to 18 V), while the computer was powered via a voltage regulator accepting 5 V. All these components were packed together on a cradle designed and manufactured to be hosted between the hexa-copter skids, benefitting also of a holder provided with an automatic attitude compensation device (part of the UAV equipment).

The overall weight was an important constraint because it influenced the duration of the flight and consequently the extension of the surveyed area. Using this light configuration the UAV was able to perform flights of at least ten minutes. Fig. 1 shows the payload mounted on the UAV.

Fig. 1. The UAV ready to take off.

B. Post processing methodology

The digital samples of the direct RHCP signal were processed to extract the sensor trajectory and to have the list of visible satellites during the data collection. Then, from the receiver trajectory, and knowing the satellites positions, we retrieved the lines of specular points on ground for the whole data collection, for each visible satellite. For details on how to calculate the specular points refer to [1] and [2].

Samples of the LHCP signal were processed to estimate the amount of reflected power, assuming the reflecting surface caused a complete flip of the signal polarization. The reflected power was estimated for all satellites in view, by evaluating the Cross Ambiguity Function (CAF) over a reduced search space and measuring the peak-to-noise-floor separation $\alpha_{mean}(1)$ [20]:

$$\alpha_{mean} = \frac{R_P}{M_c}$$

Where R_P is the value of the correlation peak, and M_c is the mean of the correlation noise, calculated from the search space obtained cross-correlating the received signal with an orthogonal code not used by the constellation. The non-coherent integration time was fixed to 10 ms. The CAF was evaluated at different rates, namely 1, 10 and 20 Hz, which corresponded to different levels of resolution along the lines of specular points.

Fig. 2 reports the peak-to-noise-floor separation, expressed in dB, for a subset of visible Pseudo-Random Noise (PRN) codes and computed at 20 Hz and smoothed with a 1st order Low Pass digital Butterworth Filter with cutoff frequency of 1 Hz. The x-axis shows the time from the beginning of the data set. It is possible to observe that the peak-to-noise-floor separation has a time-variant trend. Some epochs of the data set show values higher than 5 dB (e.g. [0–400] s), suggesting possible signal reflections, others are characterized by small values that reaches 2 dB rarely (e.g.: PRN 32 in [600 – 820] s). Differences can be noticed among satellites, as evident from 900 s to 1200 s, where values associated to PRN 3 and 19 are higher that the values of PRN 32.

IV. RESULTS AND DISCUSSION

This section presents two case studies, which have been selected to highlight different aspects and show the potential of GNSS-R using low cost hardware to monitor water surfaces on ground. The first case relates to the water detection over two lakes in Northern Italy that were taken as reference for the calibration of the sensor and of the post processing algorithms. The second case relates to smaller water surfaces, which challenge the performance of the technique in the monitoring of unexpected water contents on ground.

A. Case-Study I: Lakes

The sensor flew over the Avigliana lakes, which are large water surfaces suitable for the validation of the sensor and the post processing algorithms. The sensor passed over the lakes three times, North to South, South to North and West to East. Such passages correspond to epochs 170-230 [s], 330-390 [s] and 1560-1620 [s], in the data set that originated Fig. 2. As expected, reflections were recorded over these epochs, as reported in the zoomed view in Fig. 3, Fig. 4 and Fig. 5 respectively.

For some PRNs, the figures show that the values of the peak-to-noise-floor separation rises to approximately 10 dB and remain constant for several seconds. Such a trend is observed for those PRNs with specular points over the lakes and confirms the detection of GNSS signal reflection from the water. The duration of the reflection depends on the satellite-sensor geometry, the sensor speed and on the lake width. Indeed, as long as the specular points fall on the area covered by water, the value of the peak-to-floor separation is high, approximately several dBs. This concept can be appreciated in Fig. 6, which shows the specular points lines of all visible PRNs, superimposed to an orthophotomap. The color of the lines depends on the values of the peak-to-noise-floor separation. The black points represent the flight trajectory displayed at 1Hz rate. The colored lines represent the specular points from the 6 satellites in view that showed high values of peak-to-noise-floor separation. Boundaries between water and land can be well detected and match the orthophotomap, as visible in the zoomed view reported in Fig. 7. Focusing on the portion of land comprised between the two lakes, boundaries correspond to the sharp increases (or drops) of the peak-to-noise-floor separation along time, that were commented in Fig. 3 to 5.

Fig. 8 shows the specular points lines when the peak-to-noise-floor separation is above 6 dB. Lines are superimposed to the orthophotomap of the first lake and their extremes are linked to form a polygon. This simply represents a rough estimate of the water surface using GNSS-R. Using a shrink factor of 0.75, it turns out that the estimated circumscribed area is equal to 0.822 km^2, which is slightly less than the real water surface that is approximately 0.89 km^2.

This estimate of the water surface resulted to be approximately 7.5% less than the real value. We processed GPS reflected signals only, but the accuracy of such an estimate could be increased leveraging on multi-GNSS processing.

Working in simulation, we analyzed the benefits introduced by Galileo and GLONASS signals. Fig. 9 shows the sensor trajectory chosen for the simulation, which crosses the Northern lake almost in the middle either from North to South and from

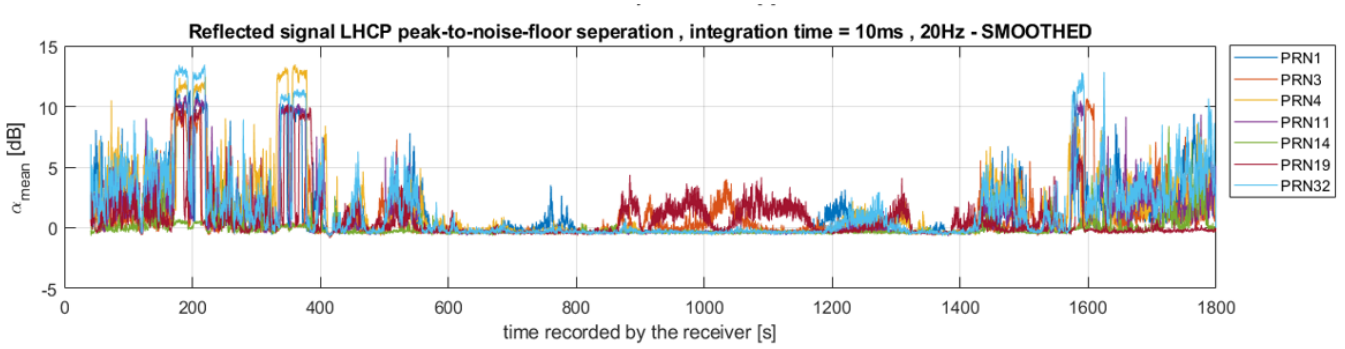

Fig. 2. Filtered peak-to-noise-floor separation of the reflected signal for a subset of visible GPS satellites.

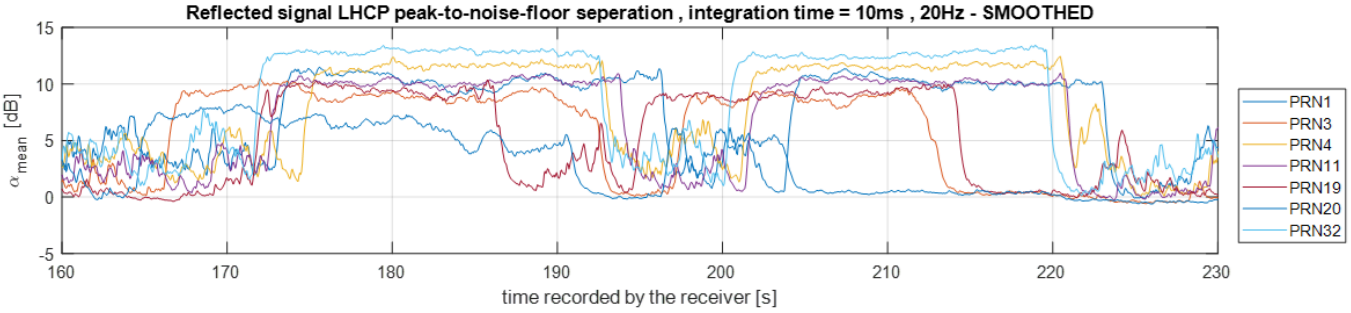

Fig. 3. Filtered peak-to-noise-floor separation of the reflected signal, when the sensor crossed the lakes from North to South.

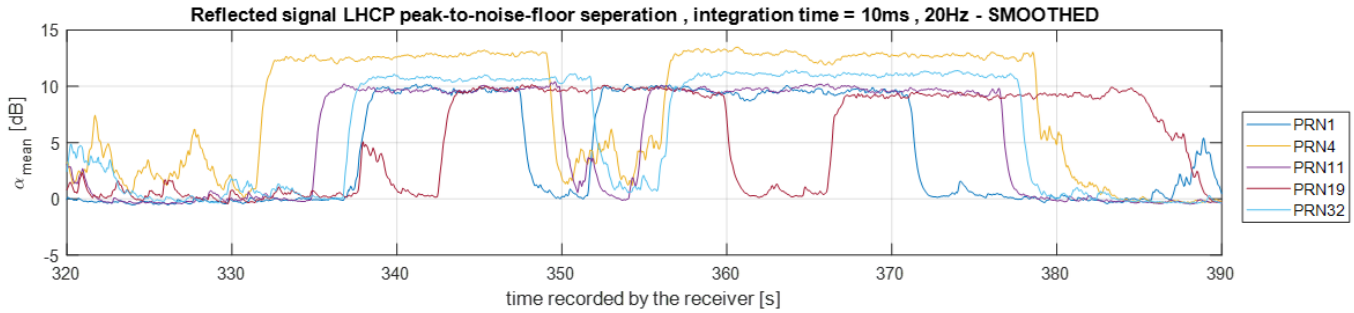

Fig. 4. Filtered peak-to-noise-floor separation of the reflected signal, when the sensor crossed the lakes from South to North.

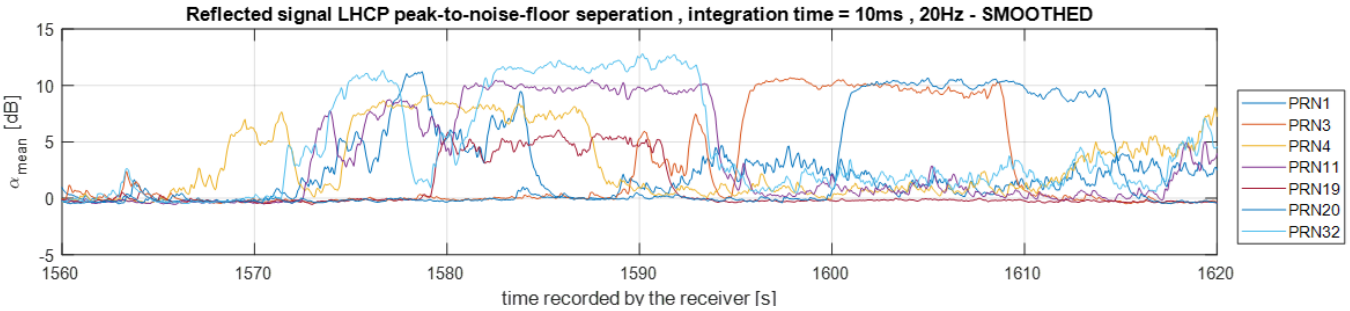

Fig. 5. Filtered peak-to-noise-floor separation of the reflected signal, when the sensor crossed the lakes from West to East.

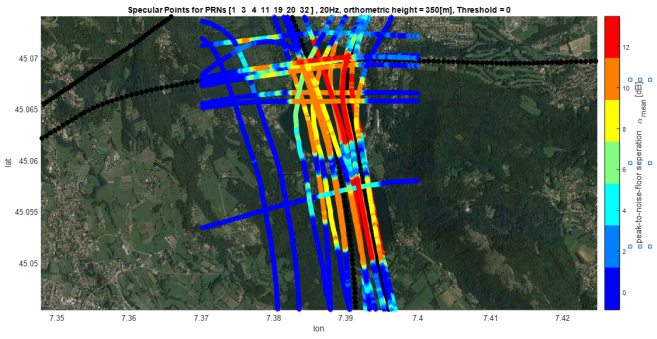

Fig. 6. GNSS signals specular reflection points overlapped to an orthophotomap, with measured reflected power indicated on colorgrades.

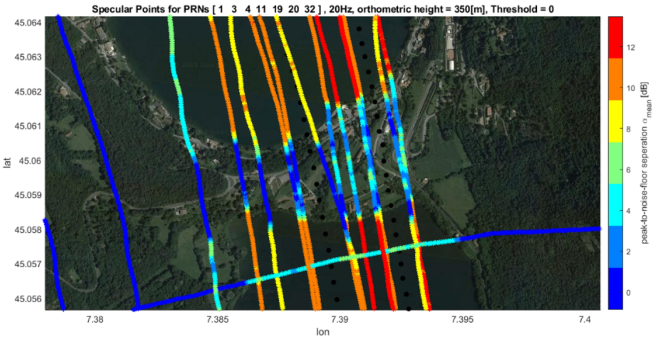

Fig. 7. Zoom view of the portion of land between the two lakes.

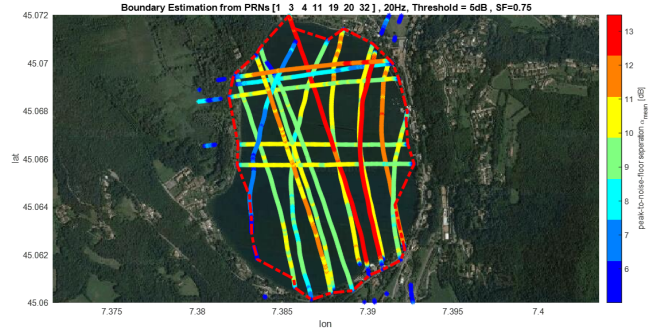

Fig. 8. Water surface estimated (red dotted line) from boundaries of reflections.

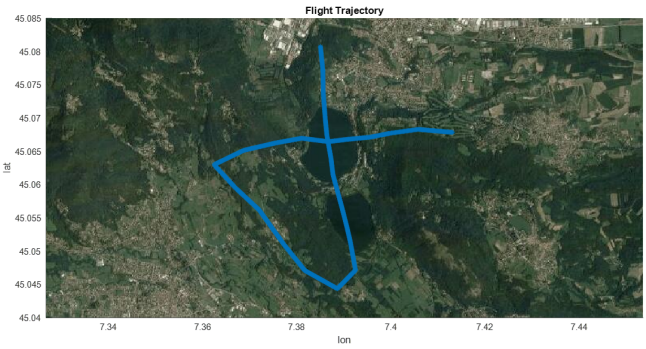

Fig. 9. Sensor trajectory considered in the water surface estimate, using processing of reflected signals from multi-GNSS.

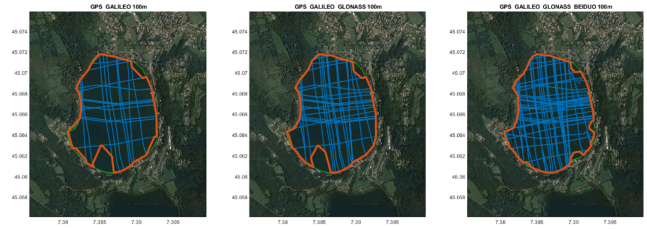

Fig. 10. Specular points lines using GPS only (left), GPS and Galileo (middle), GPS Galileo and GLONASS (right).

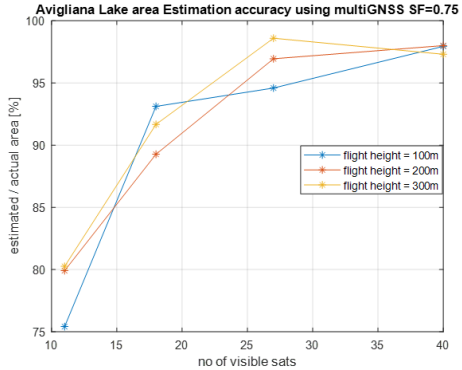

Fig. 11. Ratio between estimated and real area of the water surface versus the number of satellites in view. Three different heights of the sensor are considered.

West to East. We evaluated the reflection points lines for the satellites belonging to different constellation. We considered the selected trajectory at different heights above the Earth surface, at 100, 200 and 300 m respectively.

Fig. 10 shows a sample of the results, with a clear increment of the specular points lines as constellations are added in the simulation. For the sake of simplicity, only the case of the 100 [m] flight height is shown over the Northern lake.

The estimation performance adding multi-GNSS was also evaluated in terms of the estimation accuracy of the surface covered by the Northern lake, which was again taken as reference. Fig. 11 reports the ratio between the estimated and true area versus the number of satellites in view, which increases adding new GNSS. The estimation accuracy using GPS only remains at approximately 80% for higher heights of the sensors, but goes to 90% adding Galileo. The same metric further increases adding GLONASS, and converges to 98% if we add Beidou.

Note that multi-constellation GNSS receivers, in particular high-end receivers, can be already considered state-of-the-art for most of civil applications and they are becoming popular on board of UAVs. Although the results showed in this section refer to a specific case study (and in turn they depend on the characteristics of the water surface), they still prove the benefits one can expect from multi-GNSS in the processing

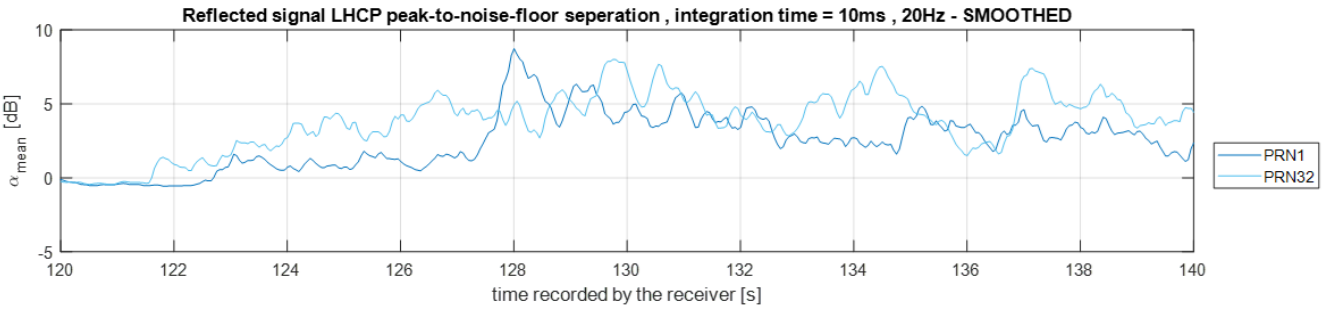

Fig. 12. Reflected signals strength when the UAV was over the river for PRN 1 and PRN 32.

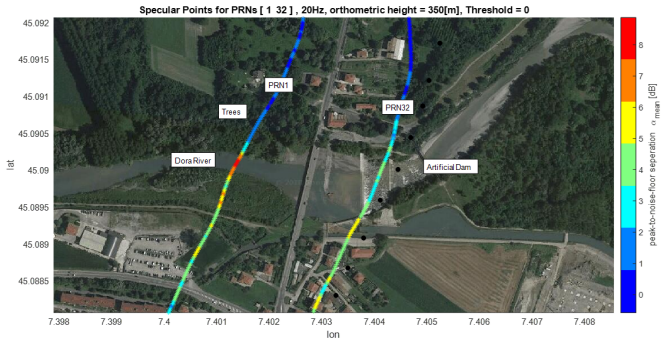

Fig. 13. Map display of the specular points over the river with reflected power indicator.

of reflected GNSS signals.

Multi-GNSS processing enables the increase of the specular reflection points over a predefined area. For instance, adding Galileo, we expect a number of satellites in view double with respect to that we could have with GPS only. At mid latitudes, adding also GLONASS and Beidou, the number of satellites in view can be higher than 40. This, in turns, increases the number of polygon vertices and results in a more accurate estimate of the water surfaces.

Clearly, the method described here is a simple and effective way to estimate water surfaces on ground, especially when maps or orthophotos are not available. Indeed, with the comparison against historic data, any expansion or shrink of the water surface can be monitored. The use of UAVs equipped with low cost GNSS-R sensors, combined with ad hoc processing routines, results to be an innovative tool for floods monitoring. The results presented here refer to specular points computed at 20 Hz, but higher resolutions are possible at the expenses of a moderated increase of the complexity burden.

B. Case-Study II: River

The second study case deals with the detection and measurement of one of the Dora river stretches, which has variable widths (dependent upon seasons) that can go from few meters to tens of meters.

The values of the peak-to-noise-floor separation for PRN 1 and PRN 32 are reported in Fig. 12. These PRNs have been selected because they show significant values in the observed time window. Following the same approach of the first study case, the specular points' lines are superimposed to the orthophotomap in Fig. 13. As in the previous case, the black dots indicate the flight trajectory at a rate of 1 Hz. The colored lines indicate the different levels of the peak-to-noise-floor separation of the reflected signals with a rate of 20Hz.

From Fig. 13, it can be appreciated the presence of a reflected signal from water, whereas boundaries between water and land match well the orthophotomap, especially those estimated by the specular points related to PRN1 (see the left part of Fig. 13). However, some differences can be noticed by observing the amount of reflected power from different satellites. Indeed, the values of the peak-to-noise-floor separation are lower for PRN32 with respect to those associated to PRN1. This is likely due to the different characteristics of the reflecting surface. While for PRN1 the specular points line crosses a stretch of the river with sharp transitions between water and land, similarly to study case 1 (i.e.: red portion in the figure), the specular points line associated to PRN32 crosses a stretch of the river after an artificial dam. Here, the water depth is low, with stones outcropping on the river level.

V. Conclusion

The results gathered in the previous sections showed the possibility to use a GNSS-based passive radar as an additional sensor of small UAVs. The prototype, built with low cost components, allowed for the collection of samples of ground-reflected GNSS signals, which revealed the presence of water surfaces on ground when post processed.

Two different study cases were investigated. Performing the data collections over lakes (and in general over large water surfaces), it was possible to detect boundaries between ground and water with a meter-level accuracy and estimate the extension of the water surface. In this case, the multi-GNSS approach (i.e.: processing of Galileo, GLONASS signals in addition to GPS) improved the estimation accuracy, with no

extra costs on the sensor hardware, but at the expenses of a moderated increase of the complexity of the software used in the off-line analysis. The data collections and the consequent signal processing demonstrated to be effective also for the detection and localization of narrower surfaces, like river stretches and small artificial basins. The experiments reported in this paper confirmed that GNSS-R is a valid alternative to conventional remote sensing technologies, such as satellite images or SAR. Indeed, GNSS-R should be considered as a valuable source of geospatial data for rescuers after floods, for UAV-based reconnaissance of remote areas and for environmental monitoring.

REFERENCES

[1] D. Gebre-Egziabher and S. Gleason, *GNSS applications and methods*. Artech House, 2009.

[2] A. Helm, "Ground-based GPS altimetry with the L1 OpenGPS receiver using carrier phase-delay observations of reflected GPS signals," Deutsches GeoForschungsZentrum GFZ, Berlin, Tech. Rep. STR 08/10, Oct. 2008.

[3] E. Vinande, D. Akos, D. Masters, P. Axelrad, and S. Esterhuizen, "GPS bistatic radar measurements of aircraft altitude and ground objects with a software receiver," in *Proceedings of the Annual Meeting - Institute of Navigation*, 2005, pp. 528–534.

[4] J. Garrison, S. Katzberg, and M. Hill, "Effect of sea roughness on bistatically scattered range coded signals from the Global Positioning System," *Geophysical Research Letters*, vol. 25, no. 13, pp. 2257–2260, 1998.

[5] E. Small, K. Larson, and J. Braun, "Sensing vegetation growth with reflected GPS signals," *Geophysical Research Letters*, vol. 37, no. 12, 2010.

[6] N. Rodriguez-Alvarez, A. Aguasca, E. Valencia, X. Bosch-Lluis, A. Camps, I. Ramos-Perez, H. Park, and M. Vall-Llossera, "Snow thickness monitoring using GNSS measurements," *IEEE Geoscience and Remote Sensing Letters*, vol. 9, no. 6, pp. 1109–1113, 2012.

[7] S. Esterhuizen, D. Masters, D. Akos, and E. Vinande, "Experimental characterization of land-reflected GPS signals," in *Proceedings of the 18th International Technical Meeting of the Satellite Division of The Institute of Navigation, ION GNSS 2005*, vol. 2005, 2005, pp. 1670–1678.

[8] Y. Pei, R. Notarpietro, P. Savi, M. Cucca, and F. Dovis, "A fully software Global Navigation Satellite System reflectometry (GNSS-R) receiver for soil monitoring," *International Journal of Remote Sensing*, vol. 35, no. 6, pp. 2378–2391, 2014.

[9] Y. Pei, R. Notarpietro, S. De Mattia, P. Savi, F. Dovis, and M. Pini, "Remote sensing of soil based on a compact and fully software GNSS-R receiver," in *26th International Technical Meeting of the Satellite Division of the Institute of Navigation, ION GNSS 2013*, vol. 1. Institute of Navigation, 2013, pp. 56–61.

[10] D. Masters, "Surface remote sensing applications of GNSS bistatic radar: Soil moisture and aircraft altimetry," Ph.D. dissertation, University of Colorado, 2004.

[11] S.-C. Wu, T. Meehan, and L. Young, "Potential use of GPS signals as ocean altimetry observables," in *Proceedings of the National Technical Meeting, Institute of Navigation*, Anon, Ed. Inst of Navigation, Alexandria, VA, United States, 1997, pp. 543–550.

[12] M. Armatys, D. Masters, A. Komjathy, P. Axelrad, and J. L. Garrison, "Exploiting GPS as a new oceanographic remote sensing tool," in *Proceedings of the 2000 National Technical Meeting of The Institute of Navigation*, Anaheim, CA, January 2000, pp. 339–347.

[13] D. Masters, S. Katzberg, and P. Axelrad, "Airborne GPS bistatic radar soil moisture measurements during SMEX02," in *International Geoscience and Remote Sensing Symposium (IGARSS)*, vol. 2, 2003, pp. 896–898.

[14] L.-C. Shen, J.-C. Juang, C.-L. Tsai, C.-C. Chang, P.-Y. Ko, and C.-L. Tseng, "Stream soil moisture estimation by reflected GPS signals with ground truth measurements," *IEEE Transactions on Instrumentation and Measurement*, vol. 58, no. 3, pp. 730–737, 2009.

[15] S. Esterhuizen and D. Akos, "The design, construction, and testing of a modular GPS bistatic radar software receiver for small platforms," Master's thesis, University of Colorado, 2006.

[16] J. Marchan-Hernandez, A. Camps, N. Rodriguez-Alvarez, X. Bosch-Lluis, I. Ramos-Perez, and E. Valencia, "PAU/GNSS-R: Implementation, performance and first results of a real-time delay-doppler map reflectometer using global navigation satellite system signals," *Sensors*, vol. 8, no. 5, pp. 3005–3019, 2008.

[17] M. Troglia Gamba, G. Marucco, M. Pini, S. Ugazio, E. Falletti, and L. Lo Presti, "Prototyping a GNSS-based passive radar for UAVs: An instrument to classify the water content feature of lands," *Sensors*, vol. 15, no. 11, pp. 28 287–28 313, 2015. [Online]. Available: http://www.mdpi.com/1424-8220/15/11/28287

[18] (2019) I-REACT project. [Online]. Available: http://www.i-react.eu/

[19] "GPS antennas, RF design considerations for u-blox GPS receivers," u-blox, Switzerland, Tech. Rep. GPS-X-08014-A1, 2009.

[20] F. Dovis, *GNSS Interference Threats and Countermeasures*. Artech House, 2015.